RESEARCH Open Access



Mandibular ramus remodeling after vertical osteotomy: a three-dimensional quantitative and qualitative assessment with sequential segmental-marrow superimposition

Sang-Hwy Lee^{1*}, Bong Chul Kim^{2*}, Hoon Cho³, Nam-Kyoo Kim³, Jong-Ki Huh⁴, Hyung Seog Yu⁵ and Sang-Hoon Kang⁶

Abstract

Background The intraoral vertical ramus osteotomy (IVRO) is a surgical technique for prognathic or asymmetric mandible. We wanted to quantitatively and qualitatively analyze the three-dimensional (3D) remodeling pattern of the mandibular ramus one year after IVRO.

Methods We reconstructed 3D mandibular models using 3D CT data from 108 IVRO hemi-mandibles of 54 subjects. The immediate postoperative (*Imm*) proximal and distal segments were separated and individually superimposed to one-year postoperative (*Post*) mandible by employing a direct segmental-isolated marrow superimposition.

Results Analysis showed extensive regional bone resorption and apposition resulting in a remodeled *Post* ramus; the more overlapping patterns of group of A (lateral type) and B (lateral/proximal type) suffered resorption-dominant remodeling compared with the less-overlapped group C (proximal type) and D (gap type), while the level of apposition was similar for all groups. *Post* ramus showed different levels of sigmoid notch filling with newly-formed bones and various shapes of new bony projections at the posterior border of the medial ramus. Bone resorption in group A was significantly and negatively correlated with protrusion delta (the difference between the postoperative and preoperative protrusive mandibular movement ranges), and bone apposition was positive with amount of postoperative maximum opening.

Conclusion All results indicate dynamic remodeling of the *Imm* ramus after IVRO in relation to the segmental overlapping pattern to form a smooth and continuous skeletal surface. The new superimposition method of direct segmental overlapping could detect the detailed remodeling pattern.

Keywords Mandible, Vertical osteotomy, Bone remodeling, Cortical bone, Superimposition

*Correspondence: Sang-Hwy Lee sanghwy@yuhs.ac Bong Chul Kim bck@wku.ac.kr

Full list of author information is available at the end of the article



© The Author(s) 2025. **Open Access** This article is licensed under a Creative Commons Attribution-NonCommercial-NoDerivatives 4.0 International License, which permits any non-commercial use, sharing, distribution and reproduction in any medium or format, as long as you give appropriate credit to the original author(s) and the source, provide a link to the Creative Commons licence, and indicate if you modified the licensed material. You do not have permission under this licence to share adapted material derived from this article or parts of it. The images or other third party material in this article are included in the article's Creative Commons licence, unless indicated otherwise in a credit line to the material. If material is not included in the article's Creative Commons licence and your intended use is not permitted by statutory regulation or exceeds the permitted use, you will need to obtain permission directly from the copyright holder. To view a copy of this licence, visit http://creativecommons.org/licenses/by-nc-nd/4.0/.

Lee et al. BMC Oral Health (2025) 25:1165 Page 2 of 17

Background

The intraoral vertical ramus osteotomy (IVRO), sometimes described as a vertical subcondylar or oblique osteotomy, is an orthognathic surgical technique for setting back the mandible [1, 2]. The mandibular distal segment, i.e., the mandibular body part anterior to ramus and condyle, is moved posteriorly after the vertical or oblique bone cut from the sigmoid notch. The distal segment overlaps the proximal segment without any fixation and becomes mobile to some extent after IVRO. Bone healing in IVRO commences in direct cortical contact with some mobility. The healing/remodeling of ramus after IVRO therefore progresses in a unique environment as compared with the conventional marrow-juxtaposed and rigidly-fixed bone healing in the sagittal split ramus osteotomy (SSRO).

SSRO is another popular surgical technique addressing mandibular movement. Though SSRO is well known for the good intersegmental bony contact, IVRO can be more advantageous in terms of reducing the risk of neurosensory disturbances, avoiding the need for rigid internal fixation and allowing passive repositioning of the condyle, which in turn contributes to a healthy temporomandibular joint [3–5]. Though IVRO is a common orthognathic procedure [3] and more advantageous [4, 5] than the popular SSRO, certain factors must be taken into consideration for clinical application such as the induction of bone healing and remodeling [1, 6]. Several studies have been conducted on the potential and outcomes

of healing, mainly based on histological findings [6–8] and radiographic images [9–13]. IVRO ramus heals in mobile cortical overlapping, which invites the primary subperiosteal/endosteal callus formation and dynamic remodeling, which in turn are strongly influenced by segmental mobility and muscular functional physiology [6–8]. However, these studies yield limited insight into how the preoperative (*Pre*) ramus can be remodeled to reshape the final postoperative (*Post*) one, especially in three dimensions (3D).

Over time, the remodeled Post ramus develops a different morphology from the original Pre and immediate postoperative (Imm) ramus, as demonstrated in Fig. 1. Post ramus (Fig. 1C) presents the remodeled ramus, with reduced ramal height, smooth contoured mandibular angle, and different condylar angulation. The difficulty in understanding the transformation of Pre (Fig. 1A) or Imm (Fig. 1B) ramus to Post ramus may be attributed to the extensive morphological and positional changes of the postsurgical segments (Fig. 1D). A few IVRO studies have reported good bone healing patterns based on 3D analysis [14], but without clear delineation of the IVRO ramus remodeling pattern [15–17]. Some other studies performed the analysis with computed tomography (CT) images for IVRO [12, 14–17], but they focused mainly on new bone formation or complicated displacements, while none examined the remodeling pattern per se.

Bone remodeling is a highly coordinated cyclic process of mature bone tissue removal by osteoclasts and new

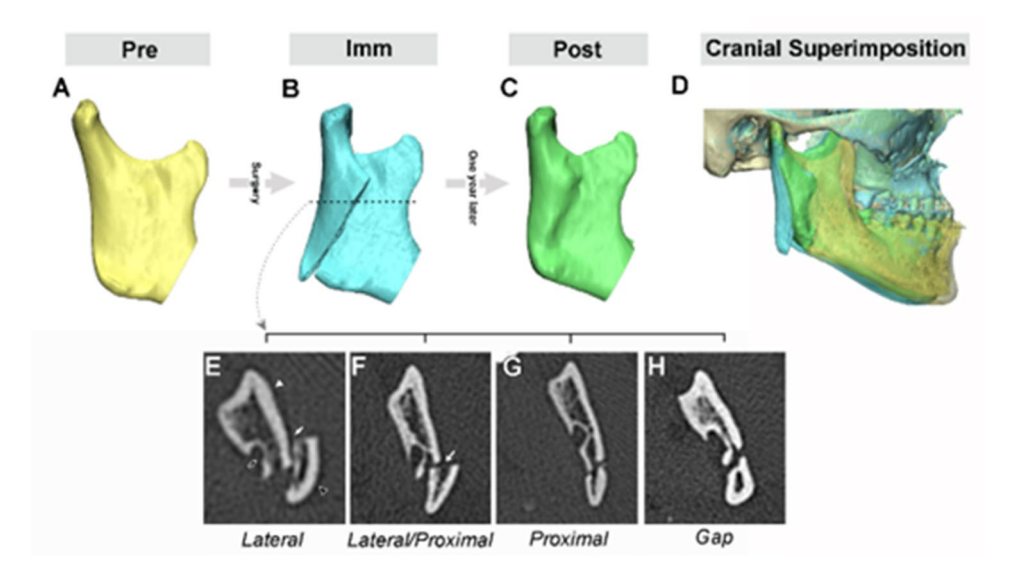


Fig. 1 Morphological and positional comparison of ramus at preoperative, immediate postoperative and one-year postoperative periods with its overlapping type at immediate postoperative stage after IVRO. The ramus was compared at three subsequent stages: (**A**) preoperative (*Pre*); (**B**) immediate postoperative (*Imm*); (**C**) one-year postoperative (*Post*); (**D**) superimposition of the three stages based on the unchanged cranial part. The overlapping patterns of the proximal segment (black arrowhead) and the distal segment (white arrowhead) in **E-H**) were evaluated at the dotted line of *Imm* ramus in (**B**) at the level of mandibular foramen on the axial images of CT data. The intersegmental area between the proximal and distal segment is indicated by a white arrow. Their overlapping patterns were classified into four types: (**E**) Lateral (for group A); (**F**) Lateral and Proximal (for group B); (**G**) Proximal (for group C); and (**H**) Gap (for group D)

Lee et al. BMC Oral Health (2025) 25:1165 Page 3 of 17

bone formation by osteoblasts [18, 19]. This process optimizes skeletal integrity by controlling the replacement of old bone [20]. It also reshapes the skeletal structure based on functional demands of mechanical loading or injuries such as fractures or IVRO. Bone remodeling therefore serves to adjust bone architecture to meet mechanical needs and/or to repair bone damage [21].

While traditional 2D imaging or experimental histological evaluations have contributed to the understanding of IVRO healing, they have fallen short in capturing the 3D geometrical complexity of *Post* mandibular remodeling. CT imaging enables the high-resolution and volumetric assessment of 3D bony morphological changes. It also allows the detailed visualization of cortical and trabecular changes necessary for skeletal analysis. CT imaging was therefore introduced to assess the dynamic 3D bone remodeling in IVRO cases.

This study aims to quantitatively and qualitatively analyze 3D remodeling of the mandibular ramus after IVRO. We hypothesized that the Imm ramus would be transformed into Post ramus via dynamic remodeling under the influence of several factors, including the Imm segmental overlapping pattern and Post mandibular function. We then postulated that the segments with more overlaps might suffer more extensive remodeling than those in groups without overlaps due to the presence of bony prominence and/or irregular surface, and that the closer segmental approximation on surgery and the active Post functional movement ranges might promote better ramal remodeling given a flat surface. We therefore wanted to investigate this remodeling by tracing 3D morphological changes from mobile Imm ramus to stable Post ramus after one year. We introduced the novel sequential superimposition methods of direct segmental and isolated marrow overlapping to avoid potential bias induced by *Post* positional and morphological changes of the proximal/distal segments.

Methods

Study design and sample

A retrospective study was designed and implemented to address the research objectives. All subjects had presented for evaluation and management of malocclusion and facial deformity, their inclusion criteria including having had bilateral IVRO for mandibular prognathism and/or asymmetry. They had undergone CT and mandibular movement range examination with the same protocol at three time points, Pre, Imm and Post for CT and at two time points, *Pre* and *Post*, for mandibular movement. Subjects were excluded if they were previously operated on, post-traumatic, syndromic, or if their treatment had been tumor-related. 108 IVRO hemi-mandibles from 54 subjects met the inclusion criteria, based on the previous reference for 3D CT study with IVRO [14]. The study consisted of 31 males and 23 females (Table 1), their ages at the time of surgery ranging between 17 and 41 years old (mean: 21.6 years old). All subjects underwent mandibular setback (mean 6.7 mm, measured at the mandibular central incisal tip of the superimposed Pre and Imm 3D model) using IVRO without any intersegmental fixation, simultaneously undergoing a Le Fort I maxillary osteotomy with semi-rigid fixation using miniplates. All subjects underwent CT examination before and after IVRO, at Pre (1-1.5 months preoperatively; mean 1.4 months), Imm (3–5 days postoperatively; mean 3.5 days), and Post (10 to 19 months; mean 12.2 months).

IVRO and *Post* management were performed for all subjects by the same protocol, including close approximation of segments by selective grinding, no intersegmental fixation, seven to ten days of intermaxillary fixation, and six to eight weeks of controlled physical therapy, i.e., staged active mandibular exercise [22, 23] for physiological bony healing and muscular rehabilitation.

Image processing and grouping by overlapping pattern

The obtained multi-detector CT data (Siemens, Somatom Definition AS+, Erlangen, Germany; FOV 200–250 mm, 512×512, pixel size 0.4–0.5 mm, 0.6 mm increment, H60s algorithm) were reconstructed to produce 3D mandibular models for the three consecutive stages of *Pre, Imm*, and *Post* using Mimics software (Version 18.0, Materialise, Leuven, Belgium) (Fig. 1A, B, C, respectively). The software was selected mainly due toits validated high registration accuracy in craniofacial imaging research [24].

Table 1 Age and gender distribution by group (groups indicating types of overlap between proximal and distal segments at the immediate postoperative stage after IVRO; total N=108)

Factors\Group*	A	В	С	D	Total	P**
Average Age	21.9	20.9	21.2	20.7	21.6	0.83 [†]
Male (sides)	38	11	5	8	62	0.13 [‡]
Female (sides)	33	7	4	2	46	
Total N (sides)	71	18	9	10	108	-
(%)	(65.7%)	(16.7%)	(8.3%)	(9.3%)	(100%)	

^{*} Group A (Lateral type), B (Lateral/Proximal type), C (Proximal), and D (Gap type)

^{**} Statistical analysis (p): by ANOVA (†); by Fisher's exact test (‡)

Lee et al. BMC Oral Health (2025) 25:1165 Page 4 of 17

The axial CT images of *Imm* ramus at the level of mandibular foramen entrance (Fig. 1B; indicated by dotted line) were used to evaluate *Imm* segment overlapping patterns between the proximal and distal segments (Fig. 1E-H). These were then categorized into 4 types, which were modified from a previous report by Kaneko et al. [14, 25]: the lateral, lateral & proximal, proximal, and gap type (Fig. 1E-H). These findings were later used to allocate the subjects into groups (the lateral as group A, lateral & proximal as group B, proximal as group C, and gap as group D) and then correlated with remodeling pattern or mandibular function.

Sequential superimposition

To implement our sequential superimposition methods, we first performed direct segmental overlapping using 3-Matic (Version 10.0, Materialise, Leuven, Belgium); *Imm* mandible (Fig. 2C) was segmented into the proximal and distal segments at the IVRO osteotomy line (Fig. 2D;

white arrowhead for the segmented *Imm* distal segment; black arrowhead for the segmented proximal segment). The *Imm* proximal segments (black arrowhead; Fig. 2D) were superimposed to *Post* mandible (Fig. 2D" and F) using point-based and morphology-based registrations [24] in software (Fig. 2B). The *Imm* distal segment (white arrowhead; Fig. 2D) was also superimposed to *Post* mandible following the same procedure (Fig. 2D" and F).

The second stage of the superimposition, isolated marrow overlapping (submitted for Korean patent 10-2024-0006750), enhanced superimposition accuracy; the outer cortical layers of mandibular proximal and distal models were removed and the mesh layers of remaining marrow were inverted with software (Mimics and 3-Matic, Materialise, Leuven, Belgium; Fig. 2G). The positions of superimposed *Imm* proximal and distal segments were then finely adjusted by following the marrow superimpositions (Fig. 2G and H). Detailed steps are provided in SFig. 1.

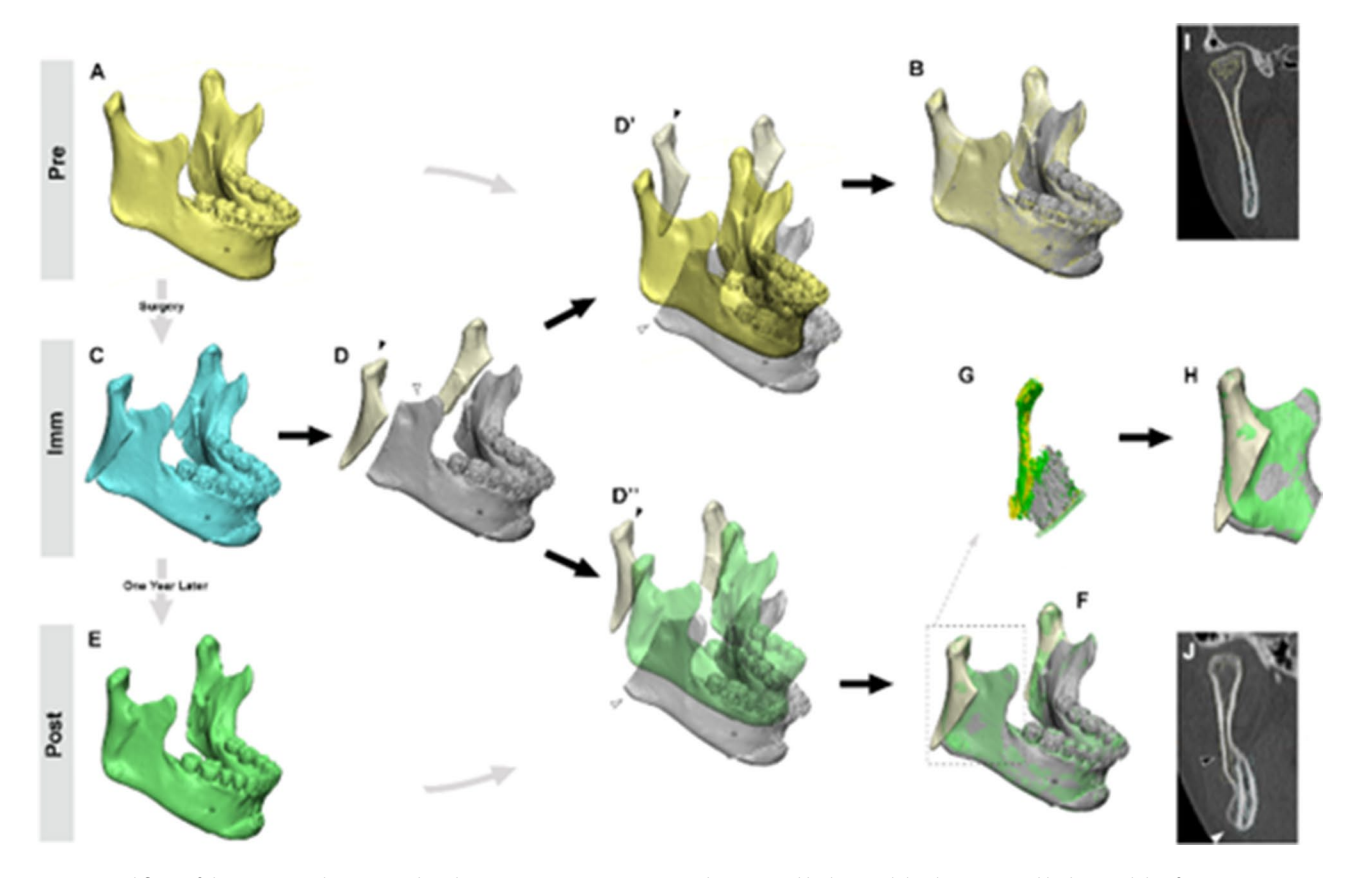


Fig. 2 Workflow of the sequential segmental and marrow superimposition with 3D mandibular models. The 3D mandibular models of (**A**) preoperative (*Pre*), (**C**) immediate postoperative (*Imm*), and (**E**) one-year postoperative (*Post*) stages were produced. (**D**) *Imm* mandible (**C**) was divided into the proximal and distal segments at the osteotomy line. (D-F) The *Imm* proximal (black arrowheads) and distal segments (white arrowheads) of (**D**) were superimposed independently by point- and surface-based registration to *Pre* mandible (**D**') for accuracy verification or to *Post* mandible (**D**') for comparison. (**G-H**) Previous superimposition was finely adjusted by the registration of the isolated marrow models of *Post* and segmented *Imm* after removing the cortical part of the models. (**I** and **J**) The coronal CT image of *Post* (**J**) or *Pre* (**I**) ramus superimposed with the segmented and superimposed *Imm* ramus for the accuracy verification. (**J**) The outline of *Imm* proximal segment is indicated by a yellow line with black arrowhead on the background of coronal *Post* CT image, and the *Imm* distal segment as a light blue line with white arrowhead. Note: proximal segment indicated by black arrowhead, distal segment by white arrowhead

Lee et al. BMC Oral Health (2025) 25:1165 Page 5 of 17

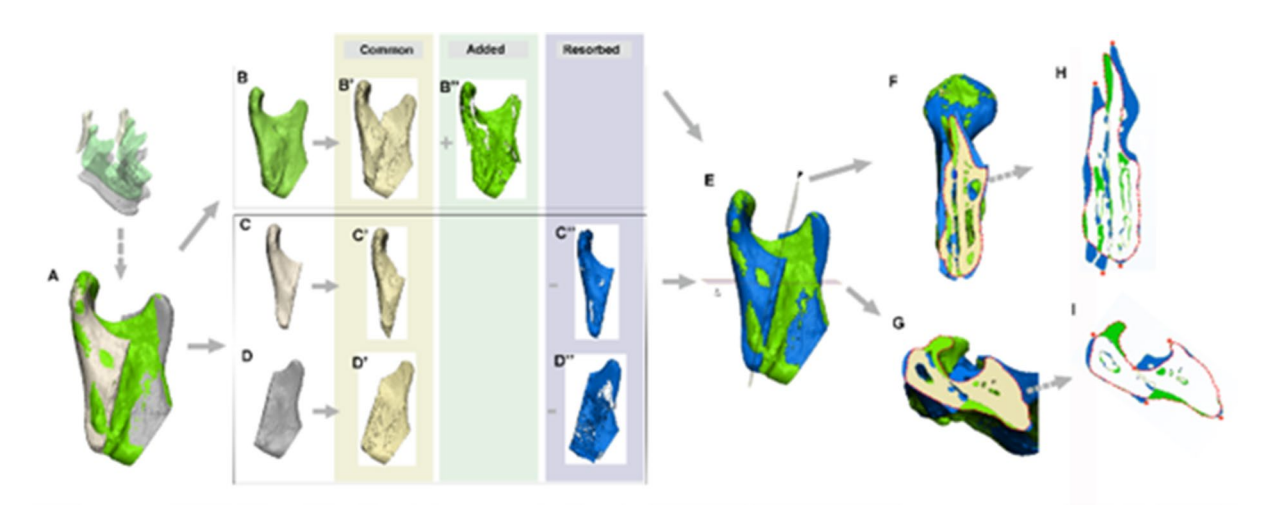


Fig. 3 The qualitative and quantitative analysis of the post-IVRO remodeling with the superimposed models. (**A**) The sequential superimpositions produced the overlapped whole *Post* and segmented *Imm* ramus. (**B-D**") The superimposed model of (**A**) could be divided into the unchanged (common), added, and resorbed part. (**E**) The superimposed model was substituted with previously divided common (in ivory), added (in light green), and resorbed (in blue) part. (**F** and **G**) The axial (indicated by white arrowhead) and coronal (indicated by black arrowhead) cutting planes were introduced to the superimposed/divided ramus of (**E**) to have the coronal cut (**F**) and axial cut (**G**) model with different colors of the origin. (**H** and **I**) The coronal and axial cut surface were achieved with their origins of the division. Note: The red dotted line of (**F-H**) indicates the original outer contour of *Post* ramus. The regional division of the coronal and axial surface was made with the red dots of each segment in (**H** and **I**) to include proximal (lateral), intersegmental, and distal (medial) regions

Quantitative and qualitative analysis of remodeled ramus

The outcome of the superimposed *Post* and *Imm* (Figs. 2H and 3A) was divided into unchanged and changed portions; *Post* mandible (Fig. 3B) could be separated into the unchanged "common" part (Fig. 3B') and added "newlyformed' part (Fig. 3B"). Similarly, *Imm* mandible (Fig. 3C and D) was divided into common parts (Fig. 3C' and D') and deleted 'resorbed' parts (Fig. 3C" and D"). The newly-formed bone in *Post* ramus was regarded as bony apposition (shown as light green in Fig. 3B" and 3E-I) and the reduced or deleted parts of *Imm* ramus as bony resorption (in blue color in Fig. 3C" and D" and 3E-I). The superimposed *Post* and *Imm* (Fig. 3A and E) was therefore regarded as mixed components of a common part (Fig. 3B, C, or D), an added part (Fig. 3B"), and two removed parts (Fig. 3C" and D").

The quantitative analysis of the remodeling was performed by measuring: 1) the 3D volume of the newlyformed and resorbed parts by subtracting the common parts from *Post* and *Imm* raumus (Fig. 3B-D"); 2) their 3D surface area as previously described (Fig. 3B-D"); 3) their 2D sectional area after getting two sectional slice images of the superimposed model (Fig. 3E-I). The third measurement of the 2D sectional area follows this protocol, the cutting planes being drawn along the osteotomy line (indicated by black arrowhead in Fig. 3E) for the coronal section (Fig. 3F and H) and at the mid-ramus (indicated by white arrowhead in Fig. 3E) for the axial section (Fig. 3G and I). The resulting models with cutting surfaces and sectional images are shown in Fig. 3F-I. The red dotted lines of Fig, 3F-I indicate the original

outer contour of *Post* mandible. The surface area measurements for the added (light green) and resorbed (blue) parts of Fig. 3H and I were made independently for the final quantification after regional division into proximal (lateral), intersegmental, and distal (medial) (with the red dots in Fig. 3H and I).

In addition, the morphological characteristics of the remodeled posterior border, sigmoid notch, and condyle were evaluated for qualitative analysis. Statistical analyses were performed to verify the association between the *Imm* segmental overlapping type or mandibular movement ranges and the ramal remodeling pattern. The R project (www.r-project.org) and Statistical Package for the Social Sciences (SPSS, v.26, IBM Co. NY, USA) were used for statistical computing.

The reproducibility of mandibular landmark using the software was also validated, as noted by Corte-Real et al. [26]. Two of the authors (Kim and Lee) marked the reference point, the mandibular foramen entrance (Fig. 1B), 10 times three and calculated their differences using Dahlberg's formula [27]. Intra- and inter-observer reliability was statistically analyzed by intra-class correlation (ICC) and technical error of measurement (TEM) with 95% confidence intervals.

Validation of method reliability

To validate the reliability of the superimposition process, we segmented 6 arbitrarily-selected *Imm* mandibles from 6 subjects into proximal and distal segments (Fig. 2D), then independently superimposed them to *Pre* mandibles of the same subjects (Fig. 2D'). This procedure

Lee et al. BMC Oral Health (2025) 25:1165 Page 6 of 17

was conducted by two authors three times at one-week intervals and the inter-surface distances measured. The intra-class correlation coefficient (ICC) was calculated to assess intra-observer and inter-observer reproducibility.

For further evaluation of reliability, *Imm* proximal and distal segments (Fig. 2D) and *Post* mandibles (Fig. 2E) from 6 randomly-selected subjects were produced. Each *Imm* mandible was superimposed to the *Post* model of the same set three times by two authors at one-week intervals, as shown in Fig. 2D" and F. The surface distance between the first, second, and third superimposed *Imm* models was measured for differences using 3-Matic, and reproducibility was statistically analyzed by calculating ICC.

We also confirmed the matching outlines of the cortical/marrow of *Imm* and *Post* ramus in the superimposition images, especially the coronal sectional view of CT images (Fig. 2J) for all cases at the end of superimposition procedures. Though the images could not be quantitatively measured for cortical and marrow outline agreement, we checked whether they coincided in terms of distance and direction, especially at the marrow trabeculae.

Results

None of the ramal remodeling-related factors were associated with the *Post* time lapse (p > 0.05; Fisher's exact test; details not shown). The right and left ramus of each subject were independently analyzed after statistical correlation analysis by Chi-squared and Fisher's exact probability tests for all outcome variables in order to exclude the possible interaction with the opposing mandible (p > 0.05; details not shown).

Fisher's statistical analysis (for gender) and analysis of variance (ANOVA) (for age) were performed to verify associations between the gender or age and the groups, i.e., the segmental overlap pattern; they showed

no significant differences among the groups (p = 0.83 for age and p = 0.13 for gender; Table 1), nor significant correlation with other ramal remodeling-related factors (p > 0.05; details not shown).

Overlapping pattern between the proximal and distal *Imm* segments

The *Imm* overlapping contact between proximal and distal segments showed four different patterns (Fig. 1E-H; Table 1). The laterally-juxtaposed proximal segment in relation to the distal segment, classified as 'Lateral' type and grouped as A (Fig. 1E), was the most frequently observed (N=71/108, 65.7%). The next frequent type was 'Lateral/Proximal,' classified as group B (16.7%; Fig. 1F), followed by the 'Gap' type (group D: 9.3%; Fig. 1H) and the 'Proximal' type (group C: 8.3%; Fig. 1G).

Ramal remodeling pattern in relation to the segmental overlapping type

The *Imm* and *Post* rami were compared quantitatively and qualitatively in each ramal region after superimposition. The *Imm* segmental overlapping types and mandibular functional ranges were then correlated with *Post* ramal remodeling.

Middle ramal region

The middle ramal overlapping region showed marked bony addition (apposition) and deletion (resorption) at the lateral and medial surfaces, resulting in complete ramal cortical continuity (Figs. 1C and 3A, and SFig. 2). The volume and areas of the 3D models or coronal-axial sections were measured individually (Tables 2, 3 and 4; STables 2 and 3). Group A and B consistently showed significantly more bone resorption than group C or D (p=0.00-0.04 for sectional area, 3D surface, and 3D volume; Table 2). However, bone apposition was not the case in that all groups, except group C, had similar

Table 2 The comparison of new bone formation and resorption measured by three measurement variables

Remodeling\\	/ariables\Group*	Α	В	С	D	p**	Bonferroni
Apposition	3D volume	1903.6±699.9	1901.4±742.3	1302.5 ± 389.5	1596.9 ± 330.8	0.05	
	3D surface area	8263.6 ± 2817.4	9441.4±3124.5	7810.6 ± 2644.0	8912.0 ± 993.5	0.32	
	Axial + Coronal [†]	72.0 ± 40.1	90.9 ± 55.0	102.8 ± 51.7	96.8 ± 36.0	0.07	
Resorption	3D volume	2065.6 ± 906.6	2365.5 ± 2046.5	1763.3 ± 866.6	1299.1 ± 451.8	0.04	
	3D surface area	8460.2 ± 2504.9	9708.2 ± 1914.3	9402.2 ± 2264.3	7123.3 ± 2255.7	0.03	B > D
	Axial + Coronal [†]	125.2 ± 46.4	117.0±45.4	53.6 ± 23.6	75.9 ± 30.6	0.00	A, B > C A > D
Sum ^{††}	3D volume	-162.1 ± 1262.7	-464.1 ± 1910.5	-460.8 ± 935.5	297.8±457.3	0.52	
	3D surface area	-196.6 ± 3622.9	-266.7 ± 2822.4	-1591.6 ± 3964.7	1788.7 ± 1804.3	0.25	
	Axial + Coronal [†]	-53.3 ±64.1	-26.2 ± 77.6	49.2±65.4	20.9 ± 53.6	0.00	C, D > A

(units: mm² for surface area and mm³ for volume)

^{*} Group A (Lateral type), B (Lateral/Proximal type), C (Proximal), and D (Gap type)

^{**} p by Kruskal-Wallis test

[†] Axial+Coronal means the addition of areas in axial and coronal sectional data in two dimensions

^{††} Sum means the subtraction of the resorption area from the apposition area, in that the positive sum value indicates more new bone formation than t resorption

Lee et al. BMC Oral Health (2025) 25:1165 Page 7 of 17

Table 3 The area measurement for new bone formation and resorption in axial and coronal section

Section\Remodeling\Group*		A	В	С	D	p**	Bonferroni
Axial	Apposition	32.7 ± 22.6	33.3 ± 16.2	19.5 ± 9.8	24.1 ± 8.2	0.10	-
	Resorption	29.2 ± 13.2	26.39 ± 11.8	17.0 ± 8.6	11.9±5.3	0.00	A, B > D A > C
	Sum [‡]	3.6 ± 24.7	6.9 ± 23.9	2.5 ± 14.2	12.2 ± 8.4	0.27	-
Coronal	Apposition	39.2 ± 29.9	57.6 ± 42.5	83.3 ± 45.9	72.7 ± 34.9	0.00	C, D > A
	Resorption	96.0 ± 39.0	90.6 ± 38.4	36.6 ± 21.5	64.0 ± 26.2	0.00	A, B > C
	Sum [‡]	-56.8 ± 52.6	-33.1 ± 61.9	46.6 ± 61.6	8.7 ± 50.8	0.00	C, D > A
Axial+Coronal [†]	Apposition	72.0 ± 40.1	90.9 ± 55.0	102.8 ± 51.7	96.8 ± 36.0	0.07	-
	Resorption	125.2 ± 46.4	117.0 ± 45.4	53.6 ± 23.6	75.9 ± 30.6	0.00	A, B > C A > D
	Sum [‡]	-53.3 ± 64.1	-26.2 ± 77.6	49.2 ± 65.4	20.9 ± 53.6	0.00	C, D > A

(units: mm²)

Table 4 The regional differences in area for new bone formation and resorption in axial plus coronal sections

Region†\Remodelii	ng∖Group [*]	Α	В	C	D	p**	Bonferroni
Proximal (lateral)	Apposition [†]	19.8 ± 17.0	14.8 ± 9.9	15.2±11.2	20.6 ± 16.2	0.78	
	Resorption [†]	71.7 ± 31.6	51.2 ± 28.0	21.6±13.9	42.4 ± 22.3	0.00	A vsC, D
Intersegmental	Apposition	38.5 ± 29.2	43.2 ± 25.0	36.3 ± 31.0	39.7 ± 26.4	0.60	
	Resorption	14.1 ± 11.2	18.6 ± 9.5	11.5 ± 6.8	11.3 ± 7.5	0.13	
Distal (medial)	Apposition	13.7 ± 21.8	32.9 ± 35.7	51.2 ± 30.3	36.5 ± 18.7	0.00	A vs. C, D
	Resorption	39.4 ± 24.0	47.2 ± 20.7	20.6 ± 17.7	22.3 ± 18.2	0.00	B vs. C, D
Total	Apposition	72.0 ± 40.1	90.9 ± 55.0	102.8 ± 51.7	96.8 ± 36.0	0.07	
	Resorption	125.2 ± 46.4	117.0 ± 45.4	53.6 ± 23.6	75.9 ± 30.6	0.00	A vs. C, D B vs. C
p**	Apposition	0.00	0.01	0.03	0.09		
Bonferroni		P vs. I, D I vs. D	P vs. I	I vs. D			
p**	Resorption	0.00	0.00	0.28	0.00		
Bonferroni		P vs. I, D I vs. D	I vs. P, D		P vs. I		

(units: mm²; measurements from axial plus coronal area)

levels for all measurement variables. The summed sectional area data (from the addition of coronal and axial area measurements) also showed resorption-dominant remodeling in group A and B while group C and D showed apposition-dominant remodeling. Among three measurement variables, the summed sectional area data presented consistent results (Table 2) and showed a significant correlation with the remaining two 3D variables (R = 0.43 - 0.75 for group A and B; STable 1). Further analyses were performed mainly with the summed sectional area data. Detailed axial and coronal area data are shown in STables 2 and 3 for reference, as well as in Table 3.

The amount of bone resorption in group A and B was greater than that of group C and D in axial, coronal, and

summed sectional areas (p = 0.00; Table 3). However, the apposition in the axial and summed sectional area was not significantly different among the groups. Moreover, the summed results of bone apposition-resorption were similar to those of bone resorption in that group C and D had more bone apposition-dominant remodeling in the coronal and summed sectional areas.

To understand regional differences in remodeling, the ramal regions in the coronal and axial sections were divided into proximal (lateral), intersegmental, and distal (medial) areas, delineated with red dots in Fig. 3H and I. The proximal (lateral) region had significantly greater resorption in group A (average 71.7 mm²) compared with group C and D (average 21.6–42.4 mm²; p=0.00;

^{*} Group A (Lateral type), B (Lateral/Proximal type), C (Proximal), and D (Gap type)

^{**} p by Kruskal-Wallis test

[†] Axial+Coronal means the addition of areas in axial and coronal sectional data

[‡] Sum means the subtraction of the resorption area from the apposition area, in that the positive sum value indicates more amount of new bone formation than that of resorption

^{*} Group A (Lateral type), B (Lateral/Proximal type), C (Proximal), and D (Gap type)

^{**} p by Kruskal-Wallis test

[†] the regions of each coronal and axial section, being divided into proximal (lateral), intersegmental, and distal (medial)(with the red dots in Fig. 3H and I)

Lee et al. BMC Oral Health (2025) 25:1165 Page 8 of 17

Table 4), but the bony apposition in the same region did not show such differences between the groups (p = 0.78). In addition, group A and B showed both apposition and resorption in the proximal (lateral) region more prominently compared with those of other regions (p = 0.00 each, except 0.01 for apposition of group B). In the distal (medial) region, apposition and resorption were again significantly different in that group C and D showed less remodeling (p = 0.00 each). The resorption and appositional areas in the intersegmental region did not differ among the groups (p = 0.6 and 0.13).

Mandibular angle region

The most prominent bone resorption was found around the angular region, mainly at the tip of the proximal segment on the lateral surface and the proximal tip of the distal segment on the medial surface (SFig. 2; indicated by black arrows). Major bone apposition, on the other hand, was found at the angular tip of the proximal segment on the medial surface (Fig. 4 with black arrows; SFig. 2 with white arrows), as will be described below in Sect. 2.4, medial new bone structure.

Sigmoid notch region

The sigmoid notch of Post ramus was analyzed as having both bone apposition and resorption (Fig. 5; Table 5); the proximal segment around the sigmoid notch mainly showed bone apposition (Fig. 5C, G, K, and O; indicated by black arrows), while the distal segment mostly had bone resorption (Fig. 5G and O; indicated by white arrows). The gap space between the proximal and distal segments at the level of the sigmoid notch was filled with newly-formed bones varying in level and shape (Fig. 5; Table 5); the majority of cases (42 sides, 59.2%) of group A showed bones filling up to the intermediate level of the two segments to form the round sigmoid notch shape (Table 5; Fig. 5M-P). Other sigmoid notch shapes included the cleft, hole, and spicule type (Fig. 5A-L; Table 5), none of the sigmoid notch shape types being significantly different among the groups (p = 0.54; Table 5).

Medial new bone structure

The medial *Post* ramus surface showed various shapes of new bone formation (Fig. 4 with black arrows). As these structures were not observed in *Imm* mandible (Fig. 4 and SFig. 2), they were regarded as newly-formed bony structure, possibly bony specular attachments for the medial pterygoid muscle. These were observed in all samples, with different shapes and sizes, and could be classified into four major types based on their morphological characteristics: ridge, single spicule, multiple spicules, and hole (Table 5; Fig. 4B, F, J, and N). In group A, 45 cases (63.4%) showed the ridge-shaped bony structure

and 17 cases (23.9%) of single spicule. The ridge type was also the most prevalent type in the other groups (60.0-77.8%), the hole and single spicule type were second-most prevalent. There were no significant differences in types of medial new structure among the groups (p = 0.56; Table 5). All the projected structures were observed to be intimately connected with the medial pterygoid muscles (indicated by the dotted line in Fig. 4D, H, L, and P).

Condylar region

The condylar region showed fewer marked bony changes than did other regions (Fig. 6; Table 6), the changes not being significantly correlated with groups (p=0.43; Table 6). 37 cases (52.1%) of group A were found to show 'minor changes,' with less than 1 mm of bony apposition or resorption (Fig. 6G-I; Table 6). 28 cases (39.4%) showed 'moderate apposition' of 1~2 mm, while only 8.5% (N=6) of group A showed apposition greater than 2 mm (Fig. 6B-E; Table 6).

The bony apposition was mainly found at the top, lateral, and/or posterior slope of the condylar head surface (as indicated by asterisk in Fig. 6C), confirmed by the double cortical outlining on the sagittal 2D CT images (Fig. 6E and indicated by an asterisk).

Mandibular movement range correlations

The functional range of mandibular movement was evaluated (STable 4) and correlated with ramal bone apposition and resorption (Table 7). Post maximum opening for groups ranged between 48.1 and 51.3 mm without significant inter-group differences (p = 0.51; STable 4 and 7), a decrease of 1.4–1.8 mm relative to the preoperative period (STable 4). Other mandibular movement-related factors, including protrusion, also showed no significant differences among groups (STable 4). Some measurement variables showed a significant correlation with bone apposition or resorption in 2D or 3D; the bone resorption in group A was significantly and negatively correlated with protrusion delta (as the difference between the *Post* and *Pre* protrusive mandibular movement range in mm) (R=-0.28, p = 0.02; Table 7). Moreover, the bone apposition for the same group was positively or negatively correlated with the amount of Post maximum opening as well as Post ipsilateral and contralateral translation (R = 0.29, -0.25, and -0.28 (or -0.24) each; Table 7). The protrusion delta was also correlated with bone apposition for group B and C (R = 0.48 and 0.77 each; Table 7).

Validation of method reproducibility

The superimposition reliability was first evaluated by measuring the mean distance in superimposed models between Imm proximal/distal segments and their corresponding Pre mandible, which was 0.04 ± 0.05 mm. Excellent evaluation reliability was obtained between

Lee et al. BMC Oral Health (2025) 25:1165 Page 9 of 17

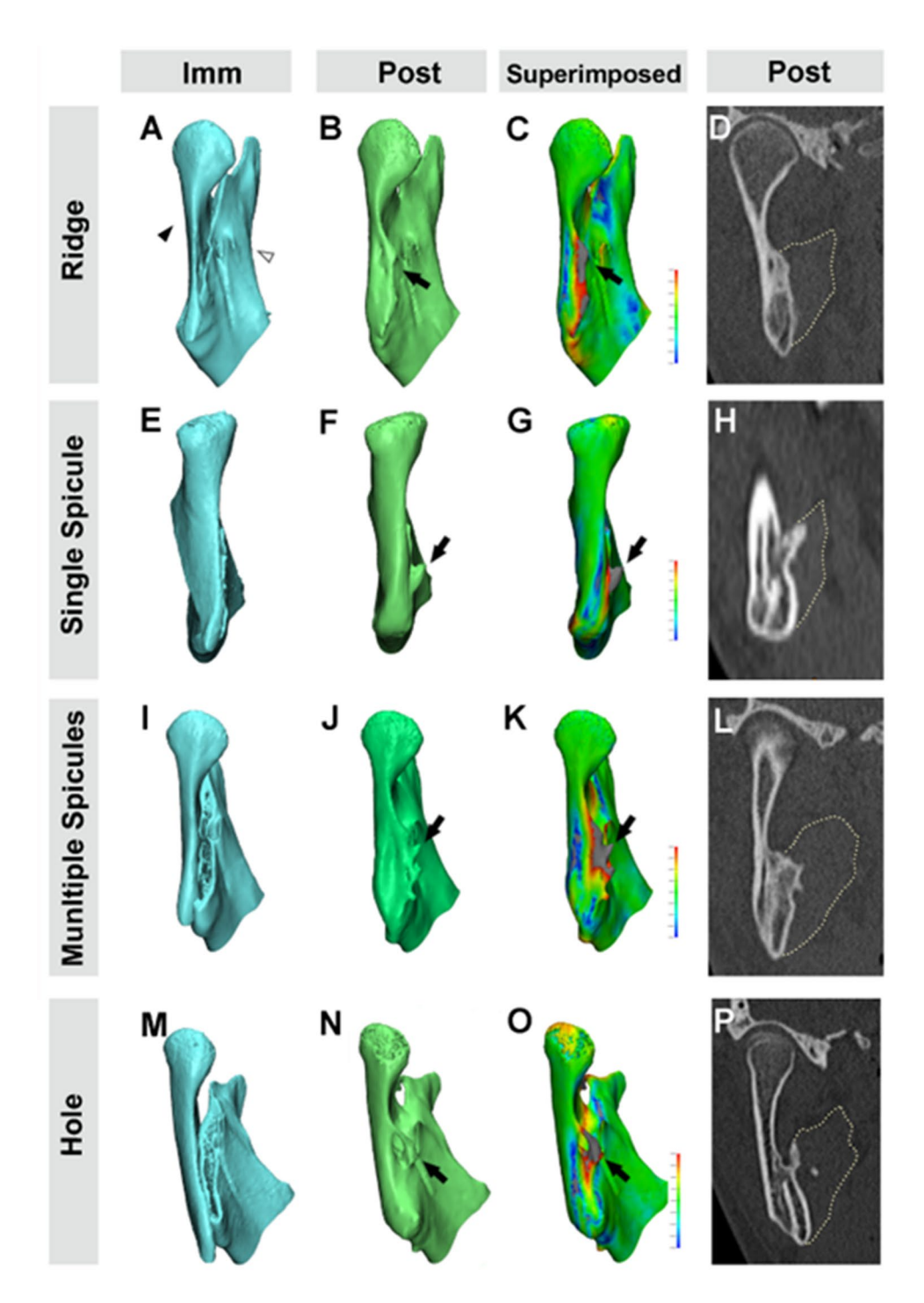


Fig. 4 The new bone structures on the medial surface of the posterior border. (**A, E, I,** and **M**) The *Imm* proximal (black arrowhead) and distal (white arrowhead) segments were completely healed and remodeled to *Post* ramus (**B, F, J**, and **N**) with the new bony structures (indicated by black arrows). (**C, G, K**, and **O**) Their superimposition was analyzed to show the inter-surface distances with a color diagram and the newly-formed structure (indicated by black arrows); these were classified into the ridge (**B-D**), single spicule (**F-H**), multiple spicules (**J-L**), or hole type (**N-P**), mainly based on their morphological characteristics. (**D, H, L**, and **P**) The dotted lines, indicating the outline of the medial pterygoid muscle, were continuous to the new bone structures of medial ramus, suggesting their relationships. Note: Color coding for **C, G, K**, and **O**: orange and red for 1.5 to 2.5 mm and gray for more than 2.5 mm of bone apposition; light and dark blue for -0.5 to -1.0 mm and in gray for more than -1.0 mm of bone resorption

Lee et al. BMC Oral Health (2025) 25:1165 Page 10 of 17

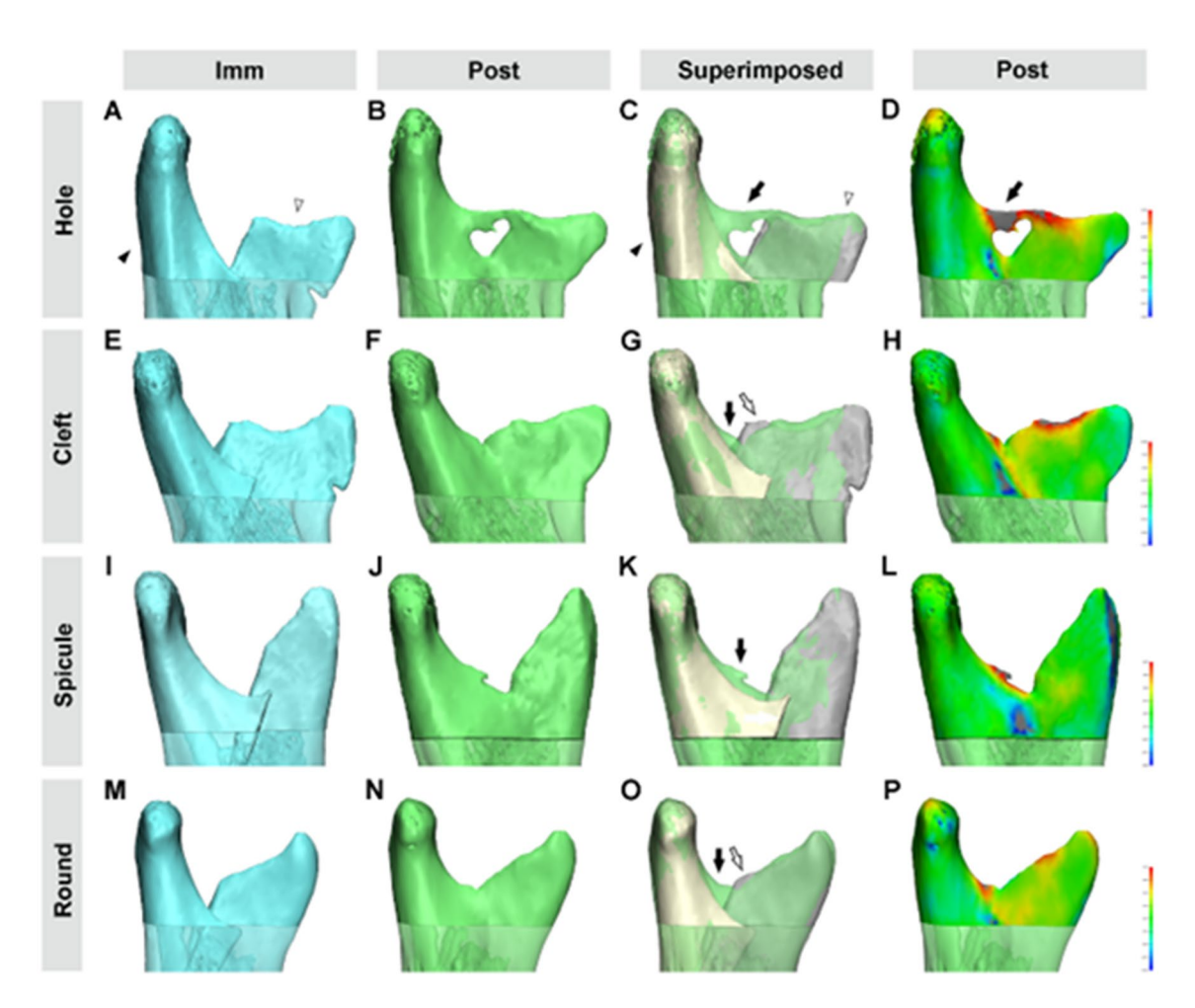


Fig. 5 Morphological comparison of immediate postoperative (*Imm*) and one-year postoperative (*Post*) sigmoid notch. The sigmoid notch of *Imm* ramus shows the bony step between the proximal and distal segments (**A**, **E**, **I** and **M**), while the *Post* sigmoid notch is continuous in contour, with different shapes (**B**, **F**, **J**, and **N**). These were classified into the hole (**B-D**), cleft (**F-H**), spicule (**J-L**), and round (**N-P**) type based on their morphological characteristics. Their superimposition was analyzed to show the inter-surface distances in color to clearly show the changed shape of the sigmoid notch (mainly indicated by black arrows). (**B-D**) These show the marked bony apposition and resorption making a bridge between the proximal and distal segments, with a hole below it; (**F-H**) The *Post* sigmoid was shaped to fill up the gap between the *Imm* proximal and distal segment, leaving a small cleft; (**J-L**) The sigmoid notch was healed to leave a small spicule; (**N-P**) The gap was filled completely to make a round-shaped sigmoid notch. Note: proximal segment, indicated by black arrowshead; distal segment by white arrowhead; bone apposition, indicated by black arrows; bone resorption, indicated by white arrows. Color coding for **D**, **H**, **L**, and **P**: orange and red for 1.5 to 2.5 mm and gray for more than 2.5 mm of bone apposition; light and dark blue for –0.5 to -1.0 mm and in gray for more than –1.0 mm of bone resorption

observers (ICC = 0.990) and within observers (ICC = 0.987 and 1.000 for observers 1 and 2).

The second evaluation was performed by measuring the surface distance between the same sets of three *Imm* mandibles, which were superimposed independently to the same sets of *Post* mandibles. Their mean distance was 0.0004 ± 0.001 mm. A good evaluation of reliability was obtained between observers (ICC = 0.768) and within observers (ICC = 0.812 and 0.924 for observers 1 and 2). A final evaluation of accuracy was made by comparing the trabecular outline of *Imm* with that of superimposed *Post*, yielding a good coincidence on the sectional images (Fig. 2J).

The reproducibility of marking the anatomical landmark (the mandibular foramen entrance) by ICC was found to be 0.972 and by relative TEM to be 1.17 mm with 95% confidence intervals.

Discussion

The primary purpose of this retrospective study was to investigate, quantitatively and qualitatively, 3D remodeling of the *Imm* ramus, which manifests segmental mobility and cortical overlap, one year after IVRO using a new segmental superimposition method. We hypothesized that *Imm* ramus is reshaped into stable *Post* ramus via dynamic remodeling in relation to the segmental overlapping pattern and mandibular function of *Imm* ramus.

Lee et al. BMC Oral Health (2025) 25:1165 Page 11 of 17

Table 5 The morphological changes at the posterior border and sigmoid Notch region in relation to intersegmental overlapping type

Region	Finding\Group [‡]	Α	В	С	D	Total	P**
Sigmoid notch shape*	Round	42	11	6	5	64	0.54
		(59.2%)	(61.1%)	(66.7%)	(50.0%)	(59.3%)	
	Cleft	18	3	2	3	26	
		(25.4%)	(16.7%)	(22.2%)	(30.0%)	(24.1%)	
	Hole	6	4	2	1	13	
		(8.5%)	(22.2%)	(22.0%)	(10.0%)	(12.0%)	
	Spicule	4	1	2	2	9	
		(5.6%)	(5.6%)	(22.2%)	(20.0%)	(8.3%)	
Medial new bone structure*	Ridge	45	12	7	6	70	0.56
		(63.4%)	(66.7%)	(77.8%)	(60.0%)	(64.5%)	
	Single spicule	17	3	3	3	26	
		(23.9%)	(16.7%)	(33.3%)	(30.0%)	(24.1%)	
	Multiple spicules	8	2	1	3	14	
		(11.3%)	(11.1%)	(11.1%)	(30.0%)	(13.0%)	
	Hole	17	4	3	0	24	
		(23.9%)	(22.2%)	(33.3%)	(0%)	(22.2%)	

Unit: N (%)

Note: Repeated counting was allowed for * marked area

^{**} statistical analysis by Fisher's exact test

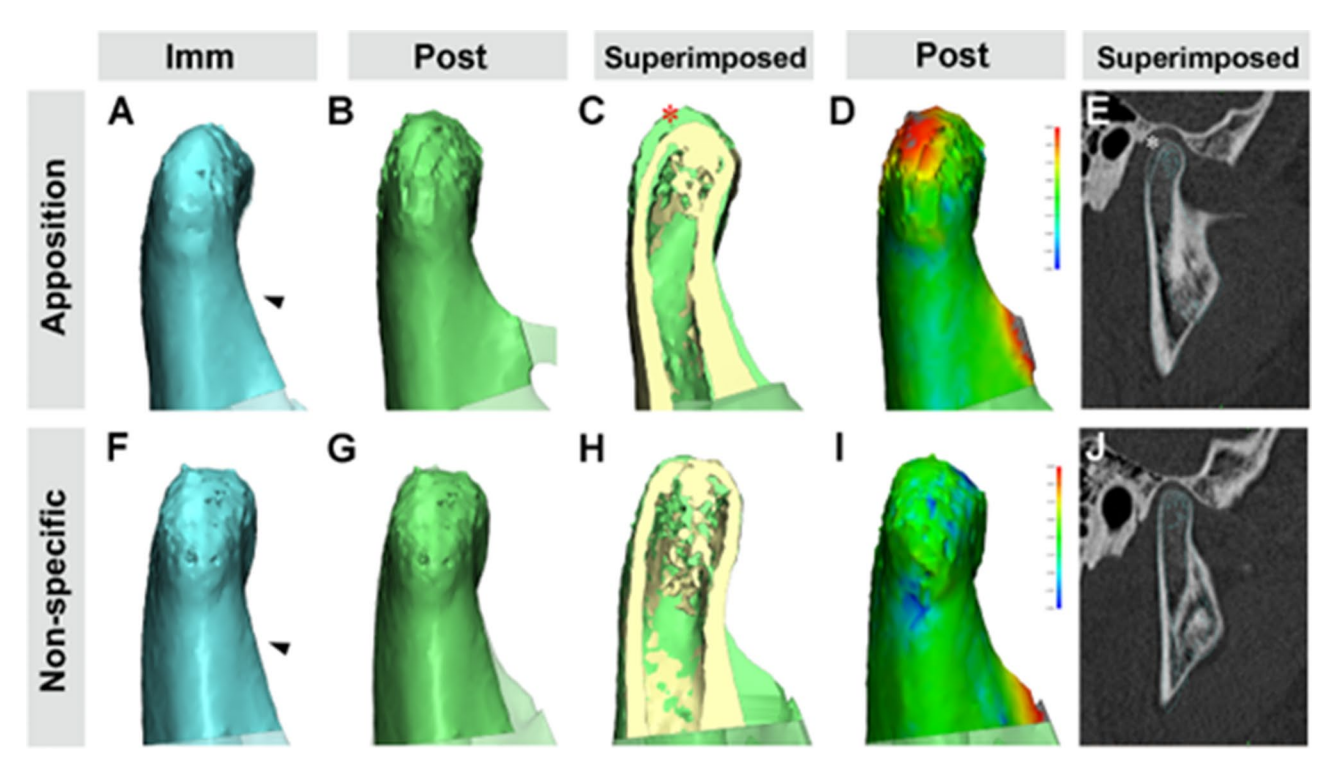


Fig. 6 Morphological comparison of immediate postoperative (*Imm*) and one-year postoperative (*Post*) condyle. The condylar head of *Imm* and *Post* period did not reveal definitive morphological or size differences (**A** and F for *Imm*; **B-D** and **G-I** for *Post*). The *Imm* condyle (indicated by the black arrowhead and ivory colored) was superimposed to *Post* condyle (light green) to reveal the *Post* remodeled ramus with different amounts of condylar bone apposition. The 3D model and sagittal CT view from *Post* (**C-E**) also show the apposition of new bone (marked by asterisk in C and E; by color diagram in **D**) or none (in **H-J**). Note: the proximal segment with the condylar head, indicated by black arrowhead; bone apposition, indicated by asterisk (*). Color coding for D and I: orange and red for 1.5 to 2.5 mm and gray for more than 2.5 mm of bone apposition; light and dark blue for –0.5 to -1.0 mm and in gray for more than – 1.0 mm of bone resorption

[‡] Group A (Lateral type), B (Lateral/Proximal type), C (Proximal), and D (Gap type)

Lee et al. BMC Oral Health (2025) 25:1165 Page 12 of 17

Table 6 The area measurements for new bone formation and resorption at the mandibular condylar head region

Region	Distance\Group [‡]	Α	В	С	D	Total	P**
Condyle	> 2 mm	6	2	0	1	9	0.43
		(8.5%)	(11.1%)	(0%)	(10.0%)	(8.3%)	
	1~2 mm	28	6	1	4	39	
		(39.4%)	(33.3%)	(11.1%)	(40.0%)	(36.1%)	
	<1 mm	37	10	8	5	60	
		(52.1%)	(55.6%)	(88.9%)	(50.0%)	(55.6%)	

Unit: N (%)

Note: * distance: the maximum distance between Pre and Post condyle around the condylion point

Table 7 The relationship between the area of bone apposition/resorption and mandibular movement ranges

Grou	p*\ Area\	Remodeling		Post max Open**	Post protrusion**	Protrusion Δ ^{††}	Post ipsi translation**	Post contra translation**
A				51.0±5.7	5.3 ± 2.4	-2.2 ± 2.7	6.7 ± 2.6	6.8 ± 2.9
	Sectional	Apposition	R^{\ddagger} p^{\dagger}	0.16 0.17	-0.01 0.97	0.09 0.47	-0.15 0.22	-0.24 0.04
		Resorption	R p [†]	-0.06 0.64	-0.08 0.50	-0.28 0.02	0.12 0.34	0.18 0.13
,	Volume	Apposition	R [‡] p [†]	0.29 0.01	-0.06 0.62	0.15 0.21	-0.25 0.04	-0.28 0.02
		Resorption	R [‡] p [†]	-0.09 0.44	-0.10 0.41	-0.19 0.11	0.00 0.10	0.02 0.85
В				51.3 ± 3.3	5.6 ± 2.0	-2.0 ± 2.6	6.9 ± 1.9	7.2 ± 1.7
	Sectional	Apposition	R^{\ddagger} p^{\dagger}	0.02 0.95	0.46 0.05	0.48 0.05	-0.20 0.42	-0.11 0.66
		Resorption	R^{\ddagger} p^{\dagger}	0.15 0.56	0.17 0.51	0.13 0.60	0.23 0.35	-0.06 0.83
,	Volume	Apposition	R [‡]	0.10 0.69	0.31 0.21	0.38 0.12	-0.10 0.69	-0.40 0.10
		Resorption	R [‡] p [†]	-0.16 0.53	-0.23 0.36	-0.09 0.73	-0.16 0.54	-0.02 0.93
C			r	48.1 ± 5.9	5.7 ± 1.4	-2.1 ± 1.5	8.6±4.2	6.8±2.6
	Sectional	Apposition	R^{\ddagger} p^{\dagger}	0.62 0.08	0.17 0.66	0.20 0.61	0.08 0.85	0.36 0.34
		Resorption	R^{\dagger} p^{\dagger}	-0.26 0.50	-0.38 0.31	-0.62 0.08	0.25 0.52	-0.18 0.64
,	Volume	Apposition	R^{\dagger} p^{\dagger}	0.24 0.53	0.45 0.23	0.77 0.02	-0.32 0.40	0.23 0.56
		Resorption	R^{\dagger} p^{\dagger}	0.70 0.04	-0.55 0.12	-0.08 0.84	-0.18 0.65	-0.39 0.30
D				49.1 ± 7.2	6.4 ± 2.5	-1.3 ± 2.2	6.9 ± 2.0	6.9 ± 2.2
	Sectional	Apposition	R^{\ddagger} p^{\dagger}	-0.42 0.23	-0.18 0.63	-0.59 0.08	-0.12 0.73	-0.31 0.38
		Resorption	R^{\ddagger} p^{\dagger}	0.27 0.45	0.34 0.33	0.11 0.76	0.04 0.92	-0.05 0.89
,	Volume	Apposition	R [‡]	0.11 0.77	0.29 0.41	-0.16 0.66	0.01 0.99	0.33 0.36
		Resorption	R [‡] p [†]	0.40 0.25	0.72 0.02	0.25 0.48	0.41 0.24	0.46 0.18

Note: * Group A (lateral type), B (lateral/proximal type), C (proximal), and D (gap type)

^{**} statistical analysis by Fisher's exact test

[‡] Group A (Lateral type), B (Lateral/Proximal type), C (Proximal), and D (Gap type)

^{**} Mandibular movement ranges in mm (mean±standard deviation); the results of mandibular movement ranges, including the maximum interincisal opening and the protrusion, were assigned to both sides of bone changes. In addition, the right and left lateral excursion data for each subject were assigned to the ipsilateral and contralateral translation so that each side had both ipsilateral and contralateral data. Details are shown in STable 4

 $[\]it tt' Protrusion Delta (\Delta): the difference between the postoperative and preoperative protrusive mandibular movement ranges (in mm; mean \pm standard deviation)$

 $[\]ddagger$ R as the correlation coefficient from a statistical analysis by Spearman's rank correlation coefficient

[†] p from the statistical analysis by Kruskal-Wallis rank sum test

Lee et al. BMC Oral Health (2025) 25:1165 Page 13 of 17

Our new analytical method, which employs sequential direct segmental and isolated marrow registration, is designed to evaluate the remodeling pattern of ramus undisturbed by the *Post* positional and morphological changes of the proximal and distal segments.

Mandibular ramal morphology, especially in mammals, consists of one angular region and two processes, forming a Y-shape. It is charged with biomechanical forces of compression and tension. The anatomical shape of the ramal bone is closely integrated with its attached masticatory muscles. The plump masticatory muscles envelop the ramus and provide stability and mobility as well as the main blood supply [28–30]. All these factors influence the extent and nature of the ramal healing and remodeling in a variety of situations such as normal growth, traumatic injury, or surgery by IVRO [5, 8].

The ramal healing is one of the main concerns after IVRO in terms of intersegmental mobility without fixation. We expect the *Imm* ramus after IVRO to be healed by subperiosteal and endosteal calluses which fill the intersegmental gap and connect the separated segments [8]. Ramal remodeling is another major concern after IVRO. Bone remodeling is a highly coordinated cyclic process of mature bone removal by osteoclasts and new bone formation by osteoblasts [18, 19]. Bone remodeling serves to adjust bone architecture to meet mechanical needs and/or to repair bone damage [21]. The ramal structure, primarily healed by calluses after IVRO, undergoes remodeling through resorption, apposition, and architectural rearrangement to meet functional and structural demands [6–8, 10–13]. However, studies have shed little light on how Imm human ramus is remodeled to Post one.

As described in the introduction, ramal remodeling studies after IVRO can be complicated by the extensive positional and morphological changes in proximal and distal segments after surgery caused by functional movement, adaptation, relapse, orthodontics, absence of intersegmental fixation and/or extensive bone remodeling/ necrosis. Thus, precise evaluation of the extent and location of the Imm segments and their interval changes over time has been difficult. For the same reasons, it was challenging to compare the Pre and Post rami to clarify the division of unchanged and changed areas. Our sequential registration method overcomes the limitations of previous studies, which utilized conventional whole mandible-based superimposition, by introducing independent segmental superimposition to avoid segmental positional change-related errors and the marrow-based second superimposition to reduce the superimposition errors by excluding the major shape changed-cortical region.

To perform a direct 3D model comparison of *Imm* and *Post* ramus, we first adopted a rigid surface-based individual segmental registration method, which utilizes the

iterative closest point algorithm after the point-based preliminary registration. Our low error level and the matching of marrow/cortex, confirmed by three steps validating method reliability, indicated the strength of this segmental superimposition method. Because *Imm* mandible after IVRO preserves a high level of segmental cortex and marrow structure as compared with SSRO mandible, the accurate and reproducible segmentation into proximal and distal segments was not so difficult. This segmental comparison seems to be a good tool for analyzing the remodeling of skeletal structures.

Moreover, our segmental registration accuracy seemed to be enhanced by the introduction of the second superimposition step, i.e., the isolated marrow registration, perhaps mainly due to the preserved skeletal structural characteristics and their limited remodeling pattern. The bone tissue consists of an outer cortex and inner marrow, both of whose spaces are rendered by the CT-based skeletal model (as seen in Fig. 3F and SFig. 1). During the first superimposition, both cortical and marrow structures can serve independently as registration references but can interfere with the process mainly due to the more dramatically changed cortical structure. The importance of the delicate architecture in marrow trabecular topology and its relative consistency during remodeling were confirmed in our isolated marrow superimposition process. To demonstrate this, we additionally dissected the segmental models into cortical and marrow parts, as shown in Fig. 2F-H and SFig. 1. These were compared using the same methods in this study (total N=20); the mean inter-surface discrepancy of the cortex in Imm-Post proximal segment was 0.57 ± 1.94 mm while that of marrow was 0.20 ± 0.39 mm (SFig. 1M and N; details not shown). Visual inspection of the sectional image also confirmed the consistent topology of the marrow trabeculae from Imm to Post ramus (Fig. 2I and J) in contrast to the marked morphological changes in the cortex region (Fig. 2H).

In this study, we learned the precise location and amount of remodeling by observing in 3D the surface differences where the proximal segment overlapped with the distal segment to produce a lateral protuberance and intersegmental space and step after IVRO. The overlapping region in particular showed extensive bone formation and resorption on both the medial and lateral surfaces, contributing to the outcome of a flat-surfaced ramus (SFig. 2 and 3). The bony remodeling at the middle ramal region varied significantly by groups, i.e., the Imm segmental overlapping types. The more the segment overlapped, as in group A and B, the more chances of bone resorption. However, the bone apposition was not significantly different among groups. Moreover, the bone apposition was pronounced at the intersegmental area of the lateral surface and the new bone structure Lee et al. BMC Oral Health (2025) 25:1165 Page 14 of 17

(as the muscular attachment) of the medial surface for all groups. The bone resorption was mainly found at the proximal segment and lateral side.

Group A and B showed strongly increased Post remodeling, being dominated by bone resorption (Tables 2 and 3). These morphological changes may account for the ramal remodeling, which produced a smooth ramal surface in these groups. *Post* rami were all covered with intact cortical outlines, their Imm intersegmental space being mainly covered with new bone; the intersegmental cortices were mostly preserved with intermittent broken regions. Group A and B rami may heal with plump subperiosteal callus while exposing the irregular ramal surface, the bony protuberances, and cutting ends without sufficient blood supply. These can lead to more active osteoclastic and less osteoblastic activity, resulting in resorption-dominant remodeling. However, Group C and D, without cortical overlap, could healed predominantly at the marrow-juxtaposed gap with endosteal calluses and a relatively plump blood supply, mimicking the approximated fracture ends. Thus the resorptive remodeling seemed to predominate at the lateral proximal regions of Group A and B. The appositional remodeling at medial ramus, where matched with the medial pterygoid attachments, implies the functional significance of mandibular movement ranges. These all support our hypothesis that Imm ramus would be dynamically remodeled under the influence of biological/mechanical factors, including the Imm segmental overlapping pattern and *Post* mandibular function. Although these findings are not studied in depth here, they parallel an animal experiment that reported the cortical outline of juxtaposed segmental cortices generally survive and can be traced [8]. We are now undertaking a follow-up study to characterize these changes in detail. These observations suggest the need for close approximation of the proximal and distal segments by selective grinding at the time of surgery to precipitate skeletal remodeling with a smoother ramal surface.

Changes observed in the angular region were similar to those of the middle ramal region, resorption at the lateral proximal segment and apposition at medial distal segments being most prominent. This remodeling pattern may be related to the protuberant high spot of the *Imm* ramus, decreased blood supply, or bone necrosis [6], as well as the resultant reduction of *Post* height of proximal segment, though not correlated with the *Imm* overlapping pattern.

The remodeled condyle showed no marked bone apposition or resorption in most cases. 8.5 and 11.1% of group A and B had bone apposition of more than 2 mm at the condylion, while most (52.1 and 55.6% each) had less than 1 mm of apposition. These data differ from previous studies, which reported 46.4% (26/56 cases) of the

remodeled condyle on CT images [15] or 80–85% of cases [31–33]. The main reason for this difference may be related partly to surgical technique and subsequent condylar displacement, but also to mistaken interpretation of a rotated condylar head in 2D radiographs [15]. Our treatment regimen, which included less condyle displacement immediately after IVRO, in association with the close approximation of proximal and distal segment as well as active functional rehabilitation, may reduce the chance of new bone formation at the condylar surface.

The range of mandibular movement, especially the protrusion and lateral excursion, was also confirmed as likely contributing to the formation of flat-surfaced Post ramus in the lateral overlapping group (Table 7 and STable 4). The skeletal muscle is functionally related to bone: its increased contraction affects the structure and biology of bone by increasing muscular vascularity, muscle mass and protein metabolism, and/or hormones/ cytokines secreted by skeletal muscle during exercise [34, 35]. Furthermore, the decreased muscular function invites increased osteoclastic activity [36, 37]. The surgical detachment of the muscles from the ramus, their rearranged envelope surrounding the ramus, and their Post functional movement ranges may also provoke the resorptive remodeling process. In addition, mandibular movement may indirectly influence bone remodeling by altering mechanical strain on the skeletal structure.

These suppositions are supported by our results, which show correlations between the protrusion delta and remodeling extent. Increased *Post* movement and lateral translations are also likely to stimulate osteoblastic activity via increased blood supply, loaded strain, and/or other biochemical actions. Though the lateral pterygoid muscle is primarily responsible for the mandibular protrusion, the masseter and medial pterygoid muscles are not only involved in the protrusive action but also control the lateral translatory movement. Our results thus suggest that the Post functional movement ranges, being controlled by medial pterygoid and masseter muscles, are correlated with the ramal remodeling, including flattening of the lateral bony overlap, the removal of bony protuberances, and the appositional bone growth at the medial muscle attachment.

A systematic exercise regimen to rehabilitate muscle tissue and skeletal function after orthognathic surgery has been emphasized [38]. These findings further support the need for *Post* active mandibular functional rehabilitation through systemic exercise, particularly in terms of protrusive and lateral movement, to precipitate skeletal remodeling with a smoother ramal surface.

As discussed previously, newly-formed structures were also observed on the medial side of the posterior border in various shapes (Fig. 4). We find no report of these bony structures after IVRO in our review of the literature.

Lee et al. BMC Oral Health (2025) 25:1165 Page 15 of 17

These new bone formations seem related to the endosteal callus and the medial pterygoid muscle since they were located just next to the osteotomy line and in intimate contact with the medial pterygoid muscle on CT images (Fig. 4D, H, L and P). The proximal/distal segments are known to have endosteal callus after IVRO [1, 8], which generally seals the open marrow surface in fracture or amputation healing [39, 40], the marrow cells being the source of endosteal callus [41]. The endosteal callus and surgically detached and physiologically reattached medial pterygoid muscle after IVRO may have interacted to form these structures [42]. This seems related to the physiological healing pattern of IVRO as well as to our treatment regimen, which includes short postsurgical intermaxillary fixation and early initiation of active physical therapy.

The retrospective design of this study may have introduced selection bias and limited control over confounding variables such as patient compliance or exact physiotherapy protocols. Nonetheless, the large sample and uniform surgical and imaging protocols mitigate some of these concerns. Future research may incorporate the tracing of *Post* segmental mobility to understand relapse-related and/or surgical movement-related positional changes, and the sectional image analysismay reveal adaptations of skeletal and soft tissue. Furthermore, the functional analysis of TMJ and prospective studies with standardized physiotherapy regimensmay clarify the optimal timing and intensity of rehabilitation for enhanced remodeling and minimized relapse.

Conclusions

We performed a direct 3D model comparative analysis of mandibular ramus from pre-operation to one year after IVRO to observe the morphological changes induced by positional changes and remodeling: from Imm ramus, in terms of segmental mobility, cortical overlap, discontinuity, and projection, to *Post* ramus with smooth-surfaced continuity and stability. We introduced the novel sequential superimposition methods of direct segmental and isolated marrow overlapping to avoid potential bias induced by Post positional and morphological changes of the proximal/distal segments. The overlapping region showed extensive bone formation and resorption at the medial and lateral surfaces, contributing to the outcome of a flat-surfaced ramus. This regional healing and remodeling were correlated with *Imm* segmental overlapping patterns and the range of mandibular movement at the middle ramus region. Moreover, new bony projections with muscular attachments were observed at the posterior border. Further evaluation of 3D positional changes of the mandible and their relationship with the remodeling pattern is planned.

Supplementary Information

The online version contains supplementary material available at https://doi.or q/10.1186/s12903-025-06567-1.

Supplementary Material 1: Supplementary Fig. 1. The isolation and superimposition of the mandibular proximal marrow models. (A-D) Imm proximal segment was divided into cortical (C) and marrow parts (D). (E-H) Post proximal segment was also separated into cortical (G) and marrow parts (H), (I-I.) Imm proximal segment was superimposed to Postramus using our segmental superimposition method (I and J), and their cortical (K) and marrow models (L) were independently compared and superimposed to adjust finely the previously performed registration with the whole cortex-marrow model. (M, N) The inter-surface distance between the marrow (M) or cortex (N) models was calculated and is shown in color maps. to reveal the high level of inter-surface distance with bony resorption (blue) and apposition (red) in the cortical models (N) and low discrepancy in marrow models (M). Note: Color coding for M: orange and red for 0.5 to 1.0 mm of bone apposition and blue for 1.0 mm of bone resorption; color coding for N: orange and red for 5.0 to 6.0 mm for bone apposition and blue for 1.0 mm of bone resorption.

Supplementary Material 2: Supplementary Fig. 2. The ramal remodeling in group A (lateral overlap) and group D (Gap). Imm ramus with the lateral overlapping type (A and D for group A; G and J for group D) was completely healed and remodeled, resulting in *Post*ramus (B and E; H and K). The *Imm* proximal (black arrowhead in A and C; ivory colored in C, F, I, and L) and distal segments (white arrowhead in A and C; gray colored in C, F, I, and L) were independently superimposed to Postramus (B and E; H and K) to reveal Postoperative remodeling (C and F; I and L). The inter-surface distance between them was calculated and is shown in color maps for the lateral (M and O) and medial side (N and P) of ramus, indicating the high level of bony apposition (blue and indicated by white arrows) and resorption (red and indicated by black arrows) mainly at the angular area. Note: Color coding for M and N: orange and red for 1.5 to 2.5 mm and gray for more than 2.5 mm of bone resorption; light and dark blue for -0.5 to -1.5 mm and in gray for more than -1.5 mm of bone apposition. Note: Color coding for O and P: in orange and red for 0.9 to 1.5 mm and in gray for more than 1.5 mm of bone resorption; in light and dark blue for -0.4 to -1.0 mm and in gray for more than -1.0 mm of bone apposition. Note: proximal segment, indicated by black arrowhead; distal segment by white arrowhead; bone apposition, indicated by white arrows; bone resorption, indicated by black arrows.

Supplementary Material 3: Supplementary Fig. 3. Summary of the ramal remodeling after IVRO.

Supplementary Material 4

Acknowledgements

We want to express sincere thanks to Professor Dr. Ji Wook Choi, Dr. Hak-Jin Kim, and Dr. Hye-Jin Tak for their valuable contributions to this paper in the areas of sampling, modeling, analysis, and statistics.

Author contributions

SHL conceived the study topic and established the experimental setup. SHL, HC, and NKK performed the experiments. BCK generated the data. All the authors analyzed and interpreted the data. SHL and BCK wrote the manuscript. All the authors read and approved the manuscript.

Funding

This work was supported by a National Research Foundation of Korea (NRF) grant funded by the Korea government (MSIT) (RS-2024-00451221). The funding bodies had no role in the design of the study, data collection, analysis, interpretation of data, or writing of the manuscript.

Data availability

The data used in this study can be made available, if required, within the regulation boundaries for data protection. They are available from the corresponding author (B. C. K.) on reasonable request.

Lee et al. BMC Oral Health (2025) 25:1165 Page 16 of 17

Declarations

Ethics approval and consent to participate

This study was performed in accordance with the guidelines of the World Medical Association Helsinki Declaration for Biomedical Research involving Human Subjects. And Wonkwang University was approved to conduct this research by the Public Institutional Review Board of South Korea (P01-202501-01-016), which waived the need for individual informed consent from the participants, whether written or verbal, owing to the non-interventional retrospective design of this study and because all data were anonymized.

Consent for publication

Not applicable.

Competing interests

The authors declare no competing interests.

Author details

¹(previous) Oral Science Research Center, Department of Oral and Maxillofacial Surgery, Yonsei University College of Dentistry, Seoul, Republic of Korea

²Department of Oral and Maxillofacial Surgery, Daejeon Dental Hospital, Wonkwang University College of Dentistry, Daejeon, Republic of Korea ³Department of Oral and Maxillofacial Surgery, Yonsei University College of Dentistry, Seoul, Republic of Korea

⁴Department of Oral and Maxillofacial Surgery, Gangnam Severance Hospital, Yonsei University College of Dentistry, Seoul, Republic of Korea ⁵Department of Orthodontics, Yonsei University College of Dentistry, Seoul, Republic of Korea

⁶Department of Oral and Maxillofacial Surgery, National Health Insurance Service Ilsan Hospital, Goyang, Republic of Korea

Received: 20 January 2025 / Accepted: 8 July 2025 Published online: 15 July 2025

References

- Boyne PJ. Osseous healing after oblique osteotomy of the mandibular Ramus. J Oral Surg (American Dent Association: 1965), 1966;24(2):125–33.
- Astrand P, Ridell A. Positional changes of the mandible and the upper and lower anterior teeth after oblique sliding osteotomy of the mandibular rami. A roentgen-cephalometric study of 55 patients. Scand J Plast Reconstr Surg. 1973;7(2):120–9.
- Ghali GE, Sikes JW Jr. Intraoral vertical Ramus osteotomy as the preferred treatment for mandibular prognathism. J Oral Maxillofacial Surgery: Official J Am Association Oral Maxillofacial Surg. 2000;58(3):313–5.
- Lee EM, Lee SH, Kim BC. Guided cutting of bone for intraoral vertical Ramus osteotomy with a freer marking technique. Br J Oral Maxillofac Surg. 2015;53(7):660–1.
- Yu TH, Lim HJ, Lee J, Kim BC. Spontaneous union of an accidentally fractured proximal segment during vertical Ramus osteotomy. J Craniofac Surg. 2017;28(4):1055–6.
- Bell WH, Kennedy JW. 3rd: Biological basis for vertical ramus osteotomies—a study of bone healing and revascularization in adult rhesus monkeys. *Journal* of oral surgery (American Dental Association: 1965) 1976, 34(3):215–224.
- Reitzik M. Cortex-to-cortex healing after mandibular osteotomy. J Oral Maxillofacial Surgery: Official J Am Association Oral Maxillofacial Surg. 1983;41(10):658–63.
- Lee SH, Park HS. Bone healing process in early mobilization after vertical Ramus osteotomy of the mandible in adult dogs. J Korean Assoc Oral Maxillofac Surg. 1997;23:434–7.
- Shepherd JP. Changes in the mandibular Ramus following osteotomy—a long-term review. Br J Oral Surg. 1980;18(3):189–201.
- Rhee BI, Park HS. On long-term remodeling of osteotomized segments after intraoral vertical Ramus osteotomy in mandibular prognathism. J Korean Assoc Oral Maxillofac Surg. 1996;22:70–85.
- Chung JH, Park HS, Hwang CJ. Morphologic and positional change of the proximal segments after intraoral vertical Ramus osteotomy of the mandibular prognathism on submentovertex cephalogram. J Korean Assoc Oral Maxillofac Surg. 2003;29:26–34.

 Nihara J, Takeyama M, Takayama Y, Mutoh Y, Saito I. Postoperative changes in mandibular prognathism surgically treated by intraoral vertical Ramus osteotomy. Int J Oral Maxillofac Surg. 2013;42(1):62–70.

- Pan JH, Lee JJ, Lin HY, Chen YJ, Jane Yao CC, Kok SH. Transverse and sagittal angulations of proximal segment after sagittal split and vertical Ramus osteotomies and their influence on the stability of distal segment. J Formos Med Association = Taiwan Yi Zhi. 2013;112(5):244–52.
- Arimoto S, Hasegawa T, Kaneko K, Tateishi C, Furudoi S, Shibuya Y, Komori T. Observation of osseous healing after intraoral vertical Ramus osteotomy: focus on computed tomography values. J Oral Maxillofacial Surgery: Official J Am Association Oral Maxillofacial Surg. 2013;71(9):e16021601–10.
- Katsumata A, Nojiri M, Fujishita M, Ariji Y, Ariji E, Langlais RP. Condylar head remodeling following mandibular setback osteotomy for prognathism: a comparative study of different imaging modalities. Oral surgery, oral medicine, oral pathology, oral radiology, and endodontics 2006, 101(4):505–14.
- Ueki K, Hashiba Y, Marukawa K, Nakagawa K, Alam S, Okabe K, Yamamoto E. The effects of changing position and angle of the proximal segment after intraoral vertical Ramus osteotomy. Int J Oral Maxillofac Surg. 2009;38(10):1041–7.
- Ohba S, Nakao N, Awara K, Tobita T, Minamizato T, Kawasaki T, Koga T, Nakatani Y, Yoshida N, Asahina I. The three-dimensional assessment of dynamic changes of the proximal segments after intraoral vertical Ramus osteotomy. Cranio: J Craniomandib Pract. 2015;33(4):276–84.
- Raggatt LJ, Partridge NC. Cellular and molecular mechanisms of bone remodeling. J Biol Chem. 2010;285(33):25103–8.
- Crockett JC, Rogers MJ, Coxon FP, Hocking LJ, Helfrich MH. Bone remodelling at a glance. J Cell Sci. 2011;124(Pt 7):991–8.
- 20. Harrigan TP, Hamilton JJ. Bone remodeling and structural optimization. J Biomech. 1994;27(3):323–8.
- 21. Hadjidakis DJ, Androulakis II. Bone remodeling. Ann N Y Acad Sci. 2006;1092:385–96.
- Bell WH. Modern practice in orthognathic and reconstructive surgery. Saunders; 1992.
- 23. Fonseca RJ, Kenny JM. Oral and maxillofacial surgery. Elsevier; 2009.
- Kim BC, Lee CE, Park W, Kang SH, Zhengguo P, Yi CK, Lee SH. Integration accuracy of digital dental models and 3-dimensional computerized tomography images by sequential point- and surface-based markerless registration. Oral surgery, oral medicine, oral pathology, oral radiology, and endodontics 2010, 110(3):370–8.
- Kaneko K, Tateishi C, Imai Y, Hasegawa T, Fukuoka Y, Furudoi S, Shibuya Y, Komori T. Observation of osseous healing after intraoral vertical Ramus osteotomy. Japanese J Jaw Deformities. 2012;22:216–22.
- Corte-Real A, Kato RM, Nunes T, Vale F, Garib D. Reproducibility of mandibular landmarks for three-dimensional assessment. Forensic Sci International: Rep. 2020;2:100144.
- Kim BC, Bertin H, Kim HJ, Kang SH, Mercier J, Perrin JP, Corre P, Lee SH. Structural comparison of hemifacial microsomia mandible in different age groups by three-dimensional skeletal unit analysis. J cranio-maxillo-facial Surgery: Official Publication Eur Association Cranio-Maxillo-Facial Surg. 2018;46(11):1875–82.
- Cohen L. Further studies into the vascular architecture of the mandible. J Dent Res. 1960;39:936–46.
- Castelli W. Vascular architecture of the human adult mandible. J Dent Res. 1963;42:786–92.
- Saka B, Wree A, Henkel KO, Anders L, Gundlach KK. Blood supply of the mandibular cortex: an experimental study in Göttingen minipigs with special reference to the condyle. J Craniomaxillofac Surg. 2002;30(1):41–5.
- Hollender L, Ridell A. Radiography of the temporomandibular joint after oblique sliding osteotomy of the mandibular Rami. Scand J Dent Res. 1974;82(6):466–9.
- Eckerdal O, Sund G, Astrand P. Skeletal remodelling in the temporomandibular joint after oblique sliding osteotomy of the mandibular Rami. Int J Oral Maxillofac Surg. 1986;15(3):233–9.
- 33. Legrell PE, Nystrom E. Radiographic study of structural changes in the temporomandibular joint after oblique sliding osteotomy: comparison between the extra-oral and intra-oral approaches. Dento Maxillo Fac Radiol. 1990;19(4):145–8.
- Karsenty G, Mera P. Molecular bases of the crosstalk between bone and muscle. Bone. 2018;115:43–9.
- Salmons S. The adaptive response of skeletal muscle: what is the evidence? Muscle Nerve. 2018;57(4):531–41.

Lee et al. BMC Oral Health (2025) 25:1165 Page 17 of 17

- 36. Zhang J, Jiao K, Zhang M, Zhou T, Liu XD, Yu SB, Lu L, Jing L, Yang T, Zhang Y, et al. Occlusal effects on longitudinal bone alterations of the temporoman-dibular joint. J Dent Res. 2013;92(3):253–9.
- Tak HJ, Moon JW, Kim JY, Kang SH, Lee SH. Transition of endochondral bone formation at the normal and botulinum-treated mandibular condyle of growing juvenile rat. Arch Oral Biol. 2024;164:105999.
- Storum KA, Bell WH. The effect of physical rehabilitation on mandibular function after Ramus osteotomies. J Oral Maxillofacial Surgery: Official J Am Association Oral Maxillofacial Surg. 1986;44(2):94–9.
- 39. Hulth A. S Olerud 1962 Studies on amputation stumps in rabbits. J Bone Joint Surg Br Volume 44-b 431–5.
- Hansen-Leth C, Reimann I. Amputations with and without myoplasty on rabbits with special reference to the vascularization. Acta Orthop Scand. 1972;43(1):68–77.
- Landry PS, Marino AA, Sadasivan KK, Albright JA. Bone injury response.
 An animal model for testing theories of regulation. Clin Orthop Relat Res. 1996;332:260–73.
- 42. Cruz DZ, Rodrigues L, Luz JG. Effects of detachment and repositioning of the medial pterygoid muscle on the growth of the maxilla and mandible of young rats. Acta Cirurgica Brasileira. 2009;24(2):93–7.

Publisher's note

Springer Nature remains neutral with regard to jurisdictional claims in published maps and institutional affiliations.